TERNARY CAHN-HILLIARD FLUIDS

JUNSEOK KIM* AND JOHN LOWENGRUB†

Abstract. In this paper, we derive a phase-field model for flows containing three (or more) liquid components. The model is based on a Navier-Stokes (NS) and Cahn-Hilliard system (CH) which accounts for surface tension among the different components and three-phase contact lines. We develop a conservative, second order accurate fully implicit discretization of the NS and three-phase (ternary) CH system that has an associated discrete energy functional. We use a nonlinear multigrid method to efficiently solve the discrete ternary CH system at the implicit time-level and then couple it to a projection method that is used to solve the NS equation. We demonstrate convergence of our scheme numerically and perform numerical simulations to show the accuracy, flexibility, and robustness of this approach. In particular, we simulate a three interface contact angle resulting from a spreading liquid lens on an interface, a buoyancy-driven compound drop, and the Rayleigh-Taylor instability of a flow with three partially miscible components.

Key words. ternary Cahn-Hilliard system, nonlinear multigrid, ternary fluid flow, interfacial tension, arbitrary miscibility

1. Introduction. Many biomedical, chemical, and industrial processes involve mixtures of three or more liquids. In spite of the importance of three-phase flows, there have been few theoretical and numerical studies of flows containing three or more liquid component compared to the large body of research for two-phase fluid flows. This is partly due to the difficulties in dealing with interfaces and triple junctions. In [26], a projection method is used for the motion of a triple junction in level set framework. In this approach, a linear projection of the level set functions onto a reduced set of variables is used to solve problems at triple lines and other multiple junctions (i.e., quadruple points). In [19], a compound drop consisting three immiscible fluids is simulated using the immersed boundary method [22]. The presence of the interface and its effect on the flow is established via source terms in the governing equations.

There are three-phase models that describe two immiscible fluids and surfactant. In [15], the effect of surfactants on the evolution of the shape of an initially nonspherical drop translating in an otherwise quiescent fluid at low Reynolds number is examined. A combination of the boundary-integral method and a finite-difference scheme is used to solve the coupled fluid dynamics and surfactant transport problems.

In this paper, we build upon on our results for two phase systems [17] to model and simulate three-phase systems. Advantages of this approach over level-set and immersed boundary approaches described above are: (1) we do not need to perform any correction steps to multiple junctions; (2) it is easy to incorporate other physical properties such as miscible and immiscible fluid components.

We derive a thermodynamically consistent system of governing equations based on a phase-field approach. The system of equations couples the Navier-Stokes equations for the fluid motion to a system of Cahn-Hilliard type (fourth order nonlinear advection-diffusion equations) for the phase variables. Here the phase fields have a definite physical meaning they are the mass ratios of the fluid components.

We develop a conservative, second order accurate fully implicit discretization of the NS and three-phase (ternary) CH system that has an associated discrete energy functional. We use a nonlinear multigrid method to efficiently solve the discrete ternary CH system at the

*Department of Mathematics 103 Multipurpose Science and Technology Building University of California, Irvine, CA 92697-3875 (jskim@math.uci.edu).

†Corresponding author. Department of Mathematics 103 Multipurpose Science and Technology Building University of California, Irvine, CA 92697-3875 (lowengrb@math.uci.edu).

implicit time-level and then couple it to a projection method that is used to solve the NS equation.

We present examples of flow with miscible and immiscible component. We demonstrate the convergence of our algorithm through a resolution study. In addition, we find good agreement with the theory for an equilibrium liquid lens (lying atop an interface). We provide demonstrations of liquid/liquid remediation. In the first example, a compound drop is simulated, in which a light fluid encapsulated a heavy contaminant drop. The light fluid causes the compound drop to rise and deposit the contaminant at an interface where it may be removed. In the second example, we investigate the diffusional transfer of a preferentially miscible contaminant from one immiscible phase to another. In this example, the transfer is enhanced by the flow and in particular the Rayleigh-Taylor instability.

The contents of this paper are as follows. In Section 2, the governing equations are derived. In Section 3, we derive the discrete scheme and numerical solution. We also present the approximate projection method used to solve the discrete generalized NS equations. Numerical experiments are presented at Section 4. In Section 5, conclusions are drawn.

2. Derivation of the governing equations. We begin by deriving a thermodynamically consistent system of governing equations for a general heterogeneous, isothermal mixture of N_f fluids following the strategy developed for binary (two component) fluids by Lowengrub and Truskinovksy [21]. Let the mass concentrations be $c_k = M_k/M$ for $k = 1, \ldots, N_f$, where M_k are the masses of the components in a representative material volume V and M is the total mass of the mixture. Since $M = \sum_{k=1}^{N_f} M_k$, we have $\sum_{k=1}^{N_f} c_k = 1$. Suppose that each component moves with a velocity $\mathbf{u}_k$ and has density $\rho_k = M_k/V_k$ where V_k is the volume of fluid k. Introducing volume fraction $\phi_k = V_k/V$, we have the relation $\rho c_k = \rho_k \phi_k$ where $\rho = \sum_{k=1}^{N_f} \rho_k \phi_k$ is the density of the mixture. Herein, we will assume that each component is incompressible, i.e. ρ_k is constant. Note that this does not mean that the mixture density ρ is constant since ρ depends on ϕ_k or, equivalently, on c_k. The relation between ρ and c_i is given by

$$\frac{1}{\rho} = \sum_{k=1}^{N_f} \frac{c_k}{\rho_k} \tag{2.1}$$

Such mixtures were termed quasi-incompressible by Lowengrub and Truskinovsky [21].

2.1. Balance equations. The balance of mass for each component is

$$\frac{\partial (\rho_k \phi_k)}{\partial t} + \nabla \cdot (\rho_k \phi_k \mathbf{u}_k) = 0. \tag{2.2}$$

Define the mass-averaged (mixture) velocity field

$$\mathbf{u} = \frac{1}{\rho} \sum_{k=1}^{N_f} \phi_k \rho_k \mathbf{u}_k = \sum_{k=1}^{N_f} c_k \mathbf{u}_k, \tag{2.3}$$

then summing Eq. (2.2) in k we obtain the balance of mass for the mixture

$$\frac{\partial \rho}{\partial t} + \nabla \cdot (\rho \mathbf{u}) = 0. \tag{2.4}$$

From Eqs. (2.2) and (2.4), we obtain the mass concentration equation:

$$\rho \dot{c}_k = \nabla \cdot \mathbf{J}_k, \tag{2.5}$$

where $\dot{} = \partial_t + \mathbf{u} \cdot \nabla$ is the advective derivative with respect to the mixture velocity, and

$$\mathbf{J}_k = -\rho c_k \mathbf{w}_k, \quad \text{where } \mathbf{w}_\mathrm{k} = (\mathbf{u}_\mathrm{k} - \mathbf{u}), \tag{2.6}$$

is the diffusion flux.

For each component, we have the balance of linear momentum

$$\rho c_k \frac{D^k \mathbf{u}_k}{Dt} = \nabla \cdot \mathbf{P}_k + \rho c_k \mathbf{g} + \pi_k, \tag{2.7}$$

where $D^k/Dt = \partial_t + \mathbf{u}_k \cdot \nabla$ is the advective derivative with respect to the component velocity, $\mathbf{P}_k$ is the stress tensor, $\mathbf{g}$ is the gravity force and π_k are the forces per unit volume due to interactions with other phases. Note that as yet $\mathbf{P}_k$ and π_k are unspecified. Summing over k, and requiring that $\sum_{k=1}^{N_f} \pi_k = 0$, which is necessary for the conservation of linear momentum of the mixture, we get the following linear momentum equation for the mixture:

$$\rho \dot{\mathbf{u}} = \nabla \cdot \mathbf{P} + \rho \mathbf{g}, \tag{2.8}$$

where $\mathbf{P} = \sum_{k=1}^{N_f} (\mathbf{P}_k - \rho c_k \mathbf{w}_k \otimes \mathbf{w}_k)$ is the stress tensor of the mixture.

Following classical theory (e.g. see [12] and Lowengrub and Truskinovsky [21]), we focus on the mixture equations and not on the detailed force interactions (e.g. π_i). Therefore, we consider an energy balance for the entire system and derive thermodynamically consistent constitutive relations for $\mathbf{P}$ and $\mathbf{J}_k$ as follows. Let Ω be an arbitrary domain that moves with the mixture velocity $\mathbf{u}$. Then, the integral form of the energy balance for the mixture is

$$\frac{d}{dt} \int_{\Omega(t)} \left(\rho e + \frac{1}{2} \rho |\mathbf{u}|^2 \right) d\Omega = \int_{\partial\Omega} \left(\mathbf{P}\mathbf{n} \cdot \mathbf{u} + \sum_{k=1}^{N_f - 1} (\mathbf{t}_k \cdot \mathbf{n}) \dot{c}_k \right) d\partial\Omega + \int_\Omega (r + \rho \mathbf{g} \cdot \mathbf{u}) \, d\Omega, \tag{2.9}$$

where e is the internal energy, $\rho|\mathbf{u}|^2/2$ is the kinetic energy and $\mathbf{n}$ is the outward normal vector to $\partial\Omega$. The first term on the right hand side is the rate of work done on $\partial\Omega$ by the fluid stress and the extra stresses due to concentration gradients, i.e. $\mathbf{t}_k$ is a generalized force that is as yet undetermined. This term is suggested by the variational analysis of Lowengrub and Truskinovsky [21]. Only $N_f - 1$ generalized forces are needed since the concentrations are not independent, i.e. $c_{N_f} = 1 - \sum_{k=1}^{N_f - 1} c_k$. In the second term on the RHS, r is the density of heat sources necessary to ensure that the temperature is constant and the remaining term is the rate of work done due to gravity.

Using the mixture mass (2.4) and momentum balance equations (2.8), local form of the energy balance Eq. (2.9) is

$$\rho \dot{e} = \mathbf{P} : \nabla \mathbf{u} + \sum_{k=1}^{N_f - 1} \nabla \cdot (\mathbf{t}_k \dot{c}_k) + r. \tag{2.10}$$

2.2. Thermodynamics and constitutive relations. Because we are dealing with isothermal flow, it is useful to introduce the Helmholtz free energy $\mathcal{F}$ rather than the internal energy. The relation between the two is

$$\mathcal{F} = e - Ts. \tag{2.11}$$

where T is the temperature. Thus, Eq. (2.10) becomes

$$\rho T \dot{s} = -\rho \dot{\mathcal{F}} + \mathbf{P} : \mathbf{u} + \sum_{i=1}^{N_f - 1} \nabla \cdot (\mathbf{t}_i \dot{c}_i) + r. \tag{2.12}$$

Next, we make the constitutive assumption that the free energy

$$\mathcal{F} = \mathcal{F}\left(c_1, \ldots, c_{N_f-1}, \nabla c_1, \ldots, \nabla c_{N_f-1}\right), \tag{2.13}$$

such that

$$\dot{\mathcal{F}} = \sum_{k=1}^{N_f-1} \left(\frac{\partial \mathcal{F}}{\partial c_k}\dot{c}_k + \frac{\partial \mathcal{F}}{\partial \nabla c_k}\left(\nabla c_k\right)^{\cdot} \right). \tag{2.14}$$

Using the identity $\left(\nabla c_k\right)^{\cdot} = \nabla \dot{c}_k - \nabla \mathbf{u} \cdot \nabla c_k$ (e.g. see [21]) and plugging Eq. (2.14) in Eq. (2.12) gives

$$\begin{aligned}\rho T \dot{s} = &\left(\mathbf{P} + \rho \sum_{k=1}^{N_f-1} \nabla c_k \otimes \frac{\partial \mathcal{F}}{\partial \nabla c_k} \right) : \nabla \mathbf{u} \\ &+ \sum_{k=1}^{N_f-1} \left(\mathbf{t}_k - \rho \frac{\partial \mathcal{F}}{\partial \nabla c_k} \right) \cdot \nabla \dot{c}_k - \rho \sum_{k=1}^{N_f-1} \left(\frac{\partial \mathcal{F}}{\partial c_k} - \frac{1}{\rho} \nabla \cdot c_k \right) \dot{c}_k + r \end{aligned} \tag{2.15}$$

Next observe that because the fluid components are incompressible the velocity gradient $\nabla \mathbf{u}$ and $\dot{c}_k$ are not independent. They are related via Eqs. (2.1) and (2.5). That is, there is a degeneracy in Eq. (2.15) since

$$\nabla \cdot \mathbf{u} = -\sum_{k=1}^{N_f-1} \frac{1}{\rho} \frac{\partial \rho}{\partial c_k} \dot{c}_k = -\sum_{k=1}^{N_f-1} \frac{1}{\rho^2} \frac{\partial \rho}{\partial c_k} \nabla \cdot \mathbf{J}_k \tag{2.16}$$

where we have used the assumption that the diffusion velocity $\mathbf{w}_i = 0$. Note that from Eq. (2.1) we have

$$-\frac{1}{\rho^2} \frac{\partial \rho}{\partial c_k} = \alpha_k \equiv \frac{1}{\rho_k} - \frac{1}{\rho_{N_f}}, \quad \text{for} \quad \mathrm{k} = 1, \ldots \mathrm{N_f} - 1, \tag{2.17}$$

is a constant. Of course if the components are density matched, $\alpha_k = 0$.

To exploit the degeneracy introduce the scalar Lagrange multiplier p. This is the mixture pressure. Then,

$$p\mathbf{I} : \nabla \mathbf{u} = \sum_{k=1}^{N_f-1} \alpha_k p \rho \dot{c}_k, \tag{2.18}$$

where $\mathbf{I}$ is the identity matrix. Using Eq. (2.18) in Eq. (2.15), we get

$$\begin{aligned}\rho T \dot{s} = &\left(\mathbf{P} + p\mathbf{I} + \rho \sum_{k=1}^{N_f-1} \nabla c_k \otimes \frac{\partial \mathcal{F}}{\partial \nabla c_k} \right) : \nabla \mathbf{u} \\ &+ \sum_{k=1}^{N_f-1} \left(\mathbf{t}_k - \rho \frac{\partial \mathcal{F}}{\partial \nabla c_k} \right) \cdot \nabla \dot{c}_k - \rho \sum_{k=1}^{N_f-1} \left(\frac{\partial \mathcal{F}}{\partial c_k} + \alpha_k p - \frac{1}{\rho} \nabla \cdot \mathbf{t}_k \right) \dot{c}_k + r. \end{aligned} \tag{2.19}$$

According to the second law of thermodynamics, in the form of the Clausius-Duhem inequality, we have

$$\rho\chi \geq 0, \qquad \text{where} \quad \rho\chi \equiv \rho \dot{\mathrm{s}} + \nabla \cdot \mathcal{J} - \mathrm{r}/\mathrm{T} \tag{2.20}$$

where χ is the internal dissipation and $\mathcal{J}$ is the entropy flux (see Truesdell and Noll [28]). Now, from Eq. (2.19) together with Eq. (2.5), we obtain

$$\rho\chi = \frac{1}{T}\left(\mathbf{P} + p\mathbf{I} + \rho\sum_{k=1}^{N_f-1}\nabla c_k \otimes \frac{\partial \mathcal{F}}{\partial \nabla c_k}\right) : \nabla\mathbf{u} + \frac{1}{T}\sum_{k=1}^{N_f-1}\left(\mathbf{t}_k - \rho\frac{\partial \mathcal{F}}{\partial \nabla c_k}\right)\cdot\nabla\left(\rho^{-1}\nabla\cdot\mathbf{J}_k\right) + \frac{1}{T}\sum_{k=1}^{N_f-1}\nabla\mu_k\cdot\mathbf{J}_k + \nabla\cdot\left(\mathcal{J} - \sum_{k=1}^{N_f-1}\frac{\mu_k J_k}{T}\right), \tag{2.21}$$

where μ_k is the generalized chemical potential given by

$$\mu_k = \frac{\partial \mathcal{F}}{\partial c_k} + \alpha_k p - \frac{1}{\rho}\nabla\cdot\mathbf{t}_k. \tag{2.22}$$

Taking the diffusion flux $\mathcal{J} = \sum_{k=1}^{N_f-1}\mu_k\mathbf{J}_k/T$ we are now in a position to pose thermodynamically consistent constitutive relations for the stress tensor $\mathbf{P}$, the forces $\mathbf{t}_k$ and the fluxes $\mathbf{J}_k$. Following Coleman and Noll [8] where $\nabla\mathbf{u}$ is varied independently from the other quantities leads to the constitutive assumptions

$$\mathbf{P} = -p\mathbf{I} - \rho\sum_{k=1}^{N_f-1}\nabla c_k\otimes\frac{\partial\mathcal{F}}{\partial\nabla c_k} + \eta\left(\mathbf{D} - \frac{2}{3}(\nabla\cdot\mathbf{u})\mathbf{I}\right), \tag{2.23}$$

$$\mathbf{t}_k = \rho\frac{\partial\mathcal{F}}{\partial\nabla c_k}, \tag{2.24}$$

$$J_k = \nu_k\nabla\mu_k, \tag{2.25}$$

where $\mathbf{D} = \left(\nabla\mathbf{u} + \nabla\mathbf{u}^T\right)$ is the rate of strain tensor and η is the viscosity (note that the bulk viscosity is assumed to be 0 for simplicity and that η may be a function of c), we obtain

$$\rho\chi = \frac{\eta}{T}\mathbf{D}:\mathbf{D} + \frac{1}{T}\sum_{k=1}^{N_f-1}\nu_k|\nabla\mu_k|^2 \geq 0 \tag{2.26}$$

and so the second law of thermodynamics is satisfied. Note that concentration gradients give rise to extra fluid stresses. As will be discussed later, these mimic surface tension stresses.

2.3. Summary of general equations. Putting together the results from the previous section, the thermodynamically consistent system of equations governing a mixture of N_f fluids is

$$\nabla\cdot\mathbf{u} = \sum_{k=1}^{N_f-1}\alpha_k\nabla\cdot\left(\nu_k\nabla\mu_k\right), \tag{2.27}$$

$$\rho\dot{\mathbf{u}} = -\nabla p - \nabla\cdot\left(\rho\sum_{k=1}^{N_f-1}\nabla c_k\otimes\frac{\partial\mathcal{F}}{\partial\nabla c_k}\right) + \nabla\cdot\left(\eta(c)\left(\mathbf{D} - \frac{2}{3}(\nabla\cdot\mathbf{u})\mathbf{I}\right)\right) + \rho\mathbf{g}, \tag{2.28}$$

$$\rho\dot{c}_k = \nabla\cdot\left(\nu_k\nabla\mu_k\right), \tag{2.29}$$

and

$$\mu_k = \frac{\partial\mathcal{F}}{\partial c_k} + \alpha_k p - \frac{1}{\rho}\nabla\cdot\left(\rho\frac{\partial\mathcal{F}}{\partial\nabla c_k}\right), \qquad \alpha_k = \frac{1}{\rho_k} - \frac{1}{\rho_{N_f}} \tag{2.30}$$

for $k = 1,\ldots,N_f-1$ and $c_{N_f} = 1 - \sum_{k=1}^{N_f-1}c_k$. This system couples a generalized Navier-Stokes equation with a nonlinear advection-diffusion equation for the concentration.

2.4. Special choice of free energy, the Navier-Stokes-Cahn-Hilliard system and nondimensionalization. To make further progress, we need to choose the form of the Helmholtz free energy. Following Cahn and Hilliard [6], we take

$$\mathcal{F} = F\left(c_1, \ldots, c_{N_f-1}\right) + \sum_{i=1}^{N_f-1} \frac{\epsilon_k^2}{4}|\nabla c_i|^2 + \frac{\epsilon_{N_f}^2}{4}|\nabla \sum_{i=1}^{N_f-1} c_i|^2, \tag{2.31}$$

where the last term is simply $\epsilon_{N_f}^2/4|\nabla c_{N_f}|^2$ written in terms of the other variables. This gives

$$\frac{\partial \mathcal{F}}{\partial \nabla c_k} = \frac{1}{2}\left(\epsilon_k^2 + \epsilon_{N_f}^2\right)\nabla c_k + \frac{\epsilon_{N_f}^2}{2}\sum_{\substack{i=1 \\ i\neq k}}^{N_f-1} \nabla c_i. \tag{2.32}$$

Note that this makes the concentration equation (2.29) a fourth order nonlinear advection diffusion equation and is a generalization of the classical Cahn-Hilliard equation used to describe phase separation in binary mixtures [6]. Further, the extra stress in the Navier-Stokes equation (2.28) can be written as

$$\rho \sum_{k=1}^{N_f-1} \nabla c_k \otimes \frac{\partial \mathcal{F}}{\partial \nabla c_k} = \rho \sum_{k=1}^{N_f} \frac{\epsilon_k^2}{2} \nabla c_k \otimes \nabla c_k, \tag{2.33}$$

where we have used that $c_{N_f} = 1 - \sum_{k=1}^{N_f-1} c_k$. The resulting system is referred to as the Navier-Stokes-Cahn-Hilliard equations (see also [21]).

We nondimensionalize the system as follows (e.g. see also [21]). Let L_* and V_* denote characteristic scales of length and velocity. Then introduce the dimensionless independent variable $\bar{x} = x/L$ and $\bar{t} = V_* t/L_*$ and the natural scaling of the dependent variables $\bar{\mathbf{u}} = \mathbf{u}/V_*$, $\bar{\rho} = \rho/\rho_*$, $\bar{\eta} = \eta/\eta_*$, $\bar{p} = p/(\rho_* V_*^2)$, $\bar{\mu}_k = \mu_k/\mu_k^*$, etc...., where again the subscripts denote characteristic quantities. The fbw is then governed by the following nondimensional parameters:

$$\begin{aligned} &\mathcal{C}_k = \frac{\epsilon_k}{L_*\sqrt{\mu_k^*}}, \quad M_k = \frac{\sigma_k/\rho_*}{\mu_k^*}, \quad Pe_k = \frac{\rho_* V_* L_*}{\nu_k^* \mu_k^*}, \\ &\mathcal{A}_k = \rho^* \alpha_k, \quad We_k = \frac{\rho_* L_* V_*^2}{\sigma_k}, \qquad Re = \frac{\rho_* V_* L_*}{\eta_*}, \quad Fr = \frac{V_*}{\sqrt{L_*|\mathbf{g}|}}, \end{aligned} \tag{2.34}$$

where the top row are the nonclassical additional parameters introduced in the model and the second row are the classical fluid dynamics parameters. In the top row, the first parameter $\mathcal{C}_k$ is the Cahn number that is a nondimensional measure of the interface energy of the kth component, the second M_k is a measure of the relative strength of the surface tension and chemical energies and the third $Pe_k$is the diffusional Peclet number that measures the relative strengths of (chemical) diffusion and advection. In the bottom row, the first parameter $\mathcal{A}_k$ is a nondimensional measure of the density differences between components, the the second We_k is the Weber number where σ_k is the phase specific surface tension (see [26] and below), the third Re is the Reynolds number that measures the relative strength of inertial and viscous forces, and finally the last Fr is the Froude number that measures the relative strengths of the inertial and gravitational forces.

Omitting the bar notation, the nondimensional Navier-Stokes-Cahn-Hilliard (NSCH)

system (2.27)-(2.30) is written as

$$\nabla \cdot \mathbf{u} = \sum_{k=1}^{N_f-1} \frac{\mathcal{A}_k}{Pe_k} \nabla \cdot (\nu_k \nabla \mu_k), \tag{2.35}$$

$$\rho \dot{\mathbf{u}} = -\nabla p - \nabla \cdot \left(\rho \sum_{k=1}^{N_f} \frac{\mathcal{C}_k^2}{M_k We_k} \nabla c_k \otimes \nabla c_k \right) + \frac{1}{Re} \nabla \cdot \left(\eta(c) \left(\mathbf{D} - \frac{2}{3} (\nabla \cdot \mathbf{u}) \mathbf{I} \right) \right) + \frac{\rho - 1}{Fr^2} \mathbf{G}, \tag{2.36}$$

$$\rho \dot{c}_k = \frac{1}{Pe_k} \nabla \cdot (\nu_k \nabla \mu_k), \tag{2.37}$$

$$\tag{2.38}$$

where we have subtracted a linear term $\rho_* \mathbf{x} \cdot \mathbf{g}$ from the pressure and $\mathbf{G} = \mathbf{g}/|\mathbf{g}|$. Further,

$$\mu_k = \frac{\partial \mathcal{F}}{\partial c_k} + \mathcal{A}_k We_k M_k p - \frac{1}{\rho} \nabla \cdot \rho \left(\frac{\mathcal{C}_k^2}{2} \nabla c_k + \frac{\mathcal{C}_{N_f}^2}{2} \sum_{i=1}^{N_f-1} \nabla c_i \right), \tag{2.39}$$

for $k = 1, \ldots, N_f - 1$.

2.5. Asymptotics and the sharp interface regime. The miscibility properties of the flow components can be described through the free energy $F(c)$. For example, if all the components are miscible the free energy is a convex function of its components (i.e. Hessian matrix is positive definite). If the components are immiscible, the free energy is a non-convex function of its components to reflect the coexistence of multiple phases. Various mixtures of miscible and immiscible components can analogously be described. When the flow components are immiscible, the NSCH system should reduce to the classical Navier-Stokes equations together with the Laplace-Young surface tension jump conditions across interfaces and multi-junctions. This requires assumptions on the nonclassical parameters $\mathcal{C}_k$, M_k and Pe_k. Following the asymptotic analyses of Lowengrub and Truskinovsky [21] and others (e.g. see the review [3]) leads to the scaling

$$\mathcal{C}_k = \epsilon^2, \qquad M_k = \epsilon/\beta \qquad \text{and } \mathrm{Pe_k} = \mathrm{O}(1) \text{ or } \mathrm{O}(1/\epsilon), \tag{2.40}$$

where the parameter ϵ is a nondimensional measure of interface thickness. Then, it can be shown that in the sharp interface limit $\epsilon \to 0$, the classical Navier-Stokes system equations and jump conditions are recovered. An interface separating two immiscible fluids has an equilibrium profile $c^{eq}(z)$ where z is the coordinate in the normal direction to the interface. The parameter β is then given by

$$\beta = \left(\int_{-\infty}^{+\infty} \rho(c^{eq}) \left(\frac{\partial c^{eq}}{\partial z} \right)^2 dz. \right)^{-1} \tag{2.41}$$

For example, with a free energy $F(c) = \frac{1}{4} c_1^2 c_2^2$, where we assume that $c_3 = 0$, then $c^{eq}(z) = \left(1 - \tanh\left(\mathrm{z}/2\epsilon\sqrt{2}\right)\right)/2$ and, if $\rho(c) = 1$, then $\beta = 6\sqrt{2}$.

Finally, following [26], the surface tension σ_{ij} between immiscible flow components i and j are decomposed into the phase-specific surface tensions σ_i and σ_j by

$$\sigma_{ij} = \sigma_i + \sigma_j \tag{2.42}$$

That is, given σ_{ij}, a linear system of equations is solved for σ_i and σ_j. The phase-specific surface tensions are used in the definition of the Weber number (2.34).

2.6. The Boussinesq approximation and the ternary system. We next consider the special case of a ternary system and use the Boussinesq approximation. In the Boussinesq approximation, the densities of the flow components are nearly matched such that $\rho \approx 1$ but the Froude number may be small enough such that $(\rho - 1)/Fr^2$ is non-negligible. Thus, in Eqs. (2.35)-(2.39), we take $\rho = 1$ except in the gravitational term and we take $\mathcal{A}_k = 0$. The resulting system is the ternary version of model H in the nomenclature of Hohenberg and Halperin [14].

The composition of a ternary mixture (A, B, and C) can be mapped onto an equilateral triangle (the Gibbs triangle [23]) whose corners represent 100% concentration of A, B or C as shown in Fig. 2.1(a). Mixtures with components lying on lines parallel to $\overline{BC}$ contain the same percentage of A, those with lines parallel to $\overline{AC}$ have the same percentage of B concentration, and analogously for the C concentration. In Fig. 2.1(a), the mixture at the position marked '$\circ$' contains 60% A, 10% B, and 30% C (The total percentage must sum to 100%).

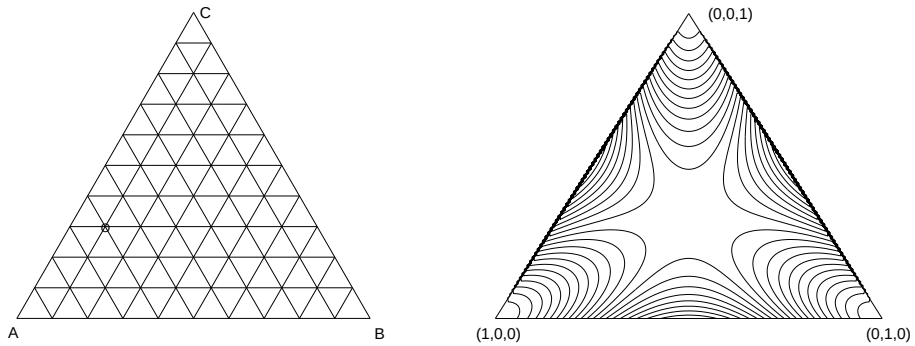

FIG. 2.1. *(a) Gibbs triangle. (b) Contour plot of the free energy* $F(\mathbf{c})$

Let $\mathbf{c} = (c_1, c_2)$ be the phase variable (i.e. concentrations of component A and component B). Since $c_1 + c_2 + c_3 = 1$ we only need to solve the equations with c_1 and c_2. Here, for simplicity, we consider a constant mobility[1] ($\nu_k \equiv 1$). $F(\mathbf{c})$ is the Helmholtz free energy which is defined on the Gibbs triangle. For three immiscible fluids, the free energy can be modeled by $F(\mathbf{c}) = \frac{1}{4}\sum_{i<j}^{3} c_i^2 c_j^2$ for the three immiscible fluids. The contours of the free energy $F(\mathbf{c})$ projected onto the Gibbs triangle are shown in Fig. 2.1(b). Note the energy minima are at the three vertices and the maximum is at the center.

[1]The extension to more general $\nu_k = \nu_k(c_1, c_2)$ is straightforward.

The non-dimensional Boussinesq ternary NSCH system is as follows:

$$\nabla \cdot \mathbf{u} = 0, \tag{2.43}$$

$$\dot{\mathbf{u}} = -\nabla p + \frac{1}{Re}\nabla \cdot (\eta(\mathbf{c})(\nabla \mathbf{u} + \nabla \mathbf{u}^T)) \tag{2.44}$$

$$-\sum_{k=1}^{3} \frac{\epsilon\beta}{We_k}\nabla \cdot (\nabla c_k \otimes \nabla c_k) + \frac{\rho - 1}{Fr^2}\mathbf{g}, \tag{2.45}$$

$$\dot{\mathbf{c}} = \frac{1}{Pe}\Delta \boldsymbol{\mu}, \tag{2.46}$$

$$\boldsymbol{\mu} = \mathbf{f}(\mathbf{c}) - \boldsymbol{\Gamma}_\epsilon \Delta \mathbf{c}, \tag{2.47}$$

where $\mathbf{f}(\mathbf{c}) = (f_1(\mathbf{c}), f_2(\mathbf{c})) = (\partial_{c_1} F(\mathbf{c}), \partial_{c_2} F(\mathbf{c}))$ and Γ_ϵ is the matrix

$$\boldsymbol{\Gamma}_\epsilon \equiv \begin{pmatrix} \epsilon^2 & \epsilon^2/2 \\ \epsilon^2/2 & \epsilon^2 \end{pmatrix}.$$

The natural boundary and initial conditions for the ternary NSCH equation are

$$\frac{\partial \mathbf{c}}{\partial n} = \frac{\partial \boldsymbol{\mu}}{\partial n} = 0, \text{ and } \quad \mathbf{u} = \mathbf{0} \quad \text{on } \partial\Omega, \qquad \mathbf{c}(\mathbf{x}, 0) = \mathbf{c}_0(\mathbf{x}), \;\; \mathbf{u}(\mathbf{x}, t) = \mathbf{0}, \tag{2.48}$$

where n is the normal unit vector pointing out of Ω.

3. Numerical Solution. The numerical solution of the ternary NSCH system uses a second-order accurate spatial discretization and a Crank-Nicholson type time stepping method. For simplicity and clarity of exposition, we will present the numerical method in 2D, but we can extend 2D to 3D straightforwardly. The computational grid consists of square cells of a uniform size h; these cells Ω_{ij} are centered at $(x_i = (i - 0.5)h,\ y_j = (j - 0.5)h)$, where $i = 1, \cdots, L$ and $j = 1, \cdots, M$. Given $\mathbf{u}^{n-1}, \mathbf{u}^n, \mathbf{c}^{n-1}, \mathbf{c}^n$, defi ned at cell centers and $p^{n-\frac{1}{2}}$ defi ned at cell corners, we want to fi nd $\mathbf{u}^{n+1}$, $\mathbf{c}^{n+1}$, and $p^{n+\frac{1}{2}}$. The outline of the algorithm is as follows:

Step 1. Initialize $\mathbf{c}^0$ to be the locally equilibrated concentration profi le and $\mathbf{u}^0$ to be the divergence-free velocity fi eld.

Step 2. Solve the CH system and update the concentration fi eld $\mathbf{c}^n$ to $\mathbf{c}^{n+1}$. We use a nonlinear Full Approximation Storage (FAS) multigrid method to solve the nonlinear discrete system (3.1) and (3.2) given below at implicit time level. The nonlinearity is treated using a nonlinear Gauss-Seidel relaxation. Details of this step are presented in our recent paper [18]. Here, however, we have additional source term due to advection. That is, we solve the following second-order accurate discrete system

$$\frac{\mathbf{c}_{ij}^{n+1} - \mathbf{c}_{ij}^n}{\Delta t} = \frac{1}{Pe}\Delta_d \boldsymbol{\mu}_{ij}^{n+\frac{1}{2}} - (\mathbf{u} \cdot \nabla_d \mathbf{c})^{n+\frac{1}{2}}, \tag{3.1}$$

$$\boldsymbol{\mu}_{ij}^{n+\frac{1}{2}} = \hat{\phi}(\mathbf{c}_{ij}^n, \mathbf{c}_{ij}^{n+1}) - \frac{1}{2}\boldsymbol{\Gamma}_\epsilon \Delta_d (\mathbf{c}_{ij}^n + \mathbf{c}_{ij}^{n+1}), \tag{3.2}$$

where Δ_d is the standard fi ve point discretization of Laplacian operator in 2D. The advection term $(\mathbf{u} \cdot \nabla_d \mathbf{c})^{n+\frac{1}{2}}$ is approximated by using a fi fth order weighted essentially non-oscillatory (WENO) scheme [16] and is described in Sec. 3.1. $\hat{\phi} = (\hat{\phi}_1, \hat{\phi}_2)$ and $\hat{\phi}_1(...)$ and $\hat{\phi}_2(...)$

denote Taylor series approximations to f_1 and f_2 up to second order, respectively:

$$\hat{\phi}_1(\mathbf{c}^n,\mathbf{c}^{n+1}) = f_1(\mathbf{c}^{n+1}) - \frac{1}{2}\partial_{c_1} f_1(\mathbf{c}^{n+1})(c_1^{n+1}-c_1^n)$$
$$-\frac{1}{2}\partial_{c_2} f_1(\mathbf{c}^{n+1})(c_2^{n+1}-c_2^n) + \frac{1}{3!}\partial_{c_1}^2 f_1(\mathbf{c}^{n+1})(c_1^{n+1}-c_1^n)^2$$
$$+\frac{2}{3!}\partial_{c_2}\partial_{c_1} f_1(\mathbf{c}^{n+1})(c_1^{n+1}-c_1^n)(c_2^{n+1}-c_2^n) + \frac{1}{3!}\partial_{c_2}^2 f_1(\mathbf{c}^{n+1})(c_2^{n+1}-c_2^n)^2$$

and

$$\hat{\phi}_2(\mathbf{c}^n,\mathbf{c}^{n+1}) = f_2(\mathbf{c}^{n+1}) - \frac{1}{2}\partial_{c_1} f_2(\mathbf{c}^{n+1})(c_1^{n+1}-c_1^n)$$
$$-\frac{1}{2}\partial_{c_2} f_2(\mathbf{c}^{n+1})(c_2^{n+1}-c_2^n) + \frac{1}{3!}\partial_{c_1}^2 f_2(\mathbf{c}^{n+1})(c_1^{n+1}-c_1^n)^2$$
$$+\frac{2}{3!}\partial_{c_2}\partial_{c_1} f_2(\mathbf{c}^{n+1})(c_1^{n+1}-c_1^n)(c_2^{n+1}-c_2^n) + \frac{1}{3!}\partial_{c_2}^2 f_2(\mathbf{c}^{n+1})(c_2^{n+1}-c_2^n)^2.$$

As described in [18], this discretization ensures that in the absence of fbw, a discrete version of Eqs. (2.46)-(2.47) is non-increasing in time independent of the choice of Δt. This gives enhanced stability.

Step 3. Update the velocity $\mathbf{u}^n$ to $\mathbf{u}^{n+1}$ and the pressure $p^{n+\frac{1}{2}}$. We use the following approximate projection method adapted from [4]. We solve

$$\frac{\mathbf{u}^*-\mathbf{u}^n}{\Delta t} = -\nabla_d p^{n-\frac{1}{2}} + \frac{1}{2Re}\nabla_d\cdot\eta(\mathbf{c}^{n+1})[\nabla_d\mathbf{u}^* + (\nabla_d\mathbf{u}^*)^T] + \frac{\rho(\mathbf{c}^{n+\frac{1}{2}})-1}{Fr^2}\mathbf{G}$$
$$+\frac{1}{2Re}\nabla_d\cdot\eta(\mathbf{c}^n)[\nabla_d\mathbf{u}^n + (\nabla_d\mathbf{u}^n)^T] + \mathbf{F}_{st}^{n+\frac{1}{2}} - (\mathbf{u}\cdot\nabla_d\mathbf{u})^{n+\frac{1}{2}} \qquad (3.3)$$

using a multigrid method for the intermediate velocity $\mathbf{u}^*$ without strictly enforcing the incompressibility constraint. We use $\mathbf{F}_{st} = \sum_{k=1}^{3}\frac{\epsilon\beta}{We_k}\nabla\cdot(|\nabla c_k|^2 I - \nabla c_k\otimes\nabla c_k)$ and the pressure fi eld is replaced by $p + \sum_{k=1}^{3}\frac{\epsilon\beta}{We_k}\nabla|\nabla c_k|^2$. The discretization of $\mathbf{F}_{st}$ is given in Sec. 3.2. The terms $\nabla_d p$ and $\nabla_d\cdot\eta(\mathbf{c})[\nabla_d\mathbf{u}+\nabla_d\mathbf{u}^T]$ are defi ned as following.

$$(\nabla_d p)_{ij} = \left(\frac{p_{i+\frac{1}{2},j+\frac{1}{2}} + p_{i+\frac{1}{2},j-\frac{1}{2}} - p_{i-\frac{1}{2},j+\frac{1}{2}} - p_{i-\frac{1}{2},j-\frac{1}{2}}}{2h},\right.$$
$$\left.\frac{p_{i+\frac{1}{2},j+\frac{1}{2}} - p_{i+\frac{1}{2},j-\frac{1}{2}} + p_{i-\frac{1}{2},j+\frac{1}{2}} - p_{i-\frac{1}{2},j-\frac{1}{2}}}{2h}\right).$$

The fi rst component of the viscous term $\nabla_d\cdot\eta(\mathbf{c})[\nabla_d\mathbf{u}+\nabla_d\mathbf{u}^T]$ is discretized as

$$\left(\nabla_d\cdot\eta(\mathbf{c})[\nabla_d\mathbf{u}+\nabla_d\mathbf{u}^T]\right)_{ij}^1 = \frac{1}{h^2}\Big(2\eta(\mathbf{c}_{i+\frac{1}{2},j})(u_{i+1,j}-u_{ij}) - 2\eta(\mathbf{c}_{i-\frac{1}{2},j})(u_{ij}-u_{i-1,j})$$
$$+\eta(\mathbf{c}_{i,j+\frac{1}{2}})(u_{i,j+1}-u_{ij}+0.25(v_{i+1,j+1}-v_{i-1,j+1}+v_{i+1,j}-v_{i-1,j}))$$
$$-\eta(\mathbf{c}_{i,j-\frac{1}{2}})(u_{ij}-u_{i,j-1}+0.25(v_{i+1,j}-v_{i-1,j}+v_{i+1,j-1}-v_{i-1,j-1}))\Big).$$

The second component of the viscous term is discretized in a similar manner. The term $(\mathbf{u}\cdot\nabla_d\mathbf{u})^{n+\frac{1}{2}}$ is computed using a fi fth order WENO scheme described in Sec. 3.1.

Then project $\mathbf{u}^*$ onto the space of approximately divergence-free vector fi elds and get the velocity $\mathbf{u}^{n+1}$, i.e., $\mathbf{u}^* = \mathbf{u}^{n+1} + \Delta t\nabla_d\phi$, where ϕ satisfi es $\Delta_d\phi = \nabla_d\cdot\frac{\mathbf{u}^*-\mathbf{u}^n}{\Delta t}$. Note $\nabla_d\cdot\mathbf{u}^{n+1}\approx 0$ see [4]. Finally, update pressure by $p^{n+\frac{1}{2}} = p^{n-\frac{1}{2}} + \phi$. This completes one time step.

3.1. Approximation of the advection terms. In this section, we describe the discretization of the advection terms. The values $\mathbf{u}_{ij}^{n+\frac{1}{2}}$ and $\mathbf{c}_{ij}^{n+\frac{1}{2}}$ are calculated using a second-order accurate extrapolation from previous values, i.e., $\mathbf{u}_{ij}^{n+\frac{1}{2}} = (3\mathbf{u}_{ij}^{n} - \mathbf{u}_{ij}^{n-1})/2$ and $\mathbf{c}_{ij}^{n+\frac{1}{2}} = (3\mathbf{c}_{ij}^{n} - \mathbf{c}_{ij}^{n-1})/2$. From these cell centered values we obtain cell edged values by $\mathbf{u}_{i+\frac{1}{2},j}^{n+\frac{1}{2}} = (\mathbf{u}_{ij}^{n+\frac{1}{2}} + \mathbf{u}_{i+1,j}^{n+\frac{1}{2}})/2$ and $\mathbf{u}_{i,j+\frac{1}{2}}^{n+\frac{1}{2}} = (\mathbf{u}_{ij}^{n+\frac{1}{2}} + \mathbf{u}_{i,j+1}^{n+\frac{1}{2}})/2$. In general, the normal velocities $u_{i+\frac{1}{2},j}^{n+\frac{1}{2}}$ and $v_{i,j+\frac{1}{2}}^{n+\frac{1}{2}}$ at the edges are not divergence-free. To reduce the overall error, we apply the MAC projection [25] before construction of the convective derivatives. The equation

$$\Delta_d \phi = \nabla_{MAC} \cdot \mathbf{u}^{n+\frac{1}{2}} \tag{3.4}$$

is solved for a cell centered ϕ, where

$$(\nabla_{MAC} \cdot \mathbf{u}^{n+\frac{1}{2}})_{ij} = \frac{u_{i+\frac{1}{2},j}^{n+\frac{1}{2}} - u_{i-\frac{1}{2},j}^{n+\frac{1}{2}}}{h} + \frac{v_{i,j+\frac{1}{2}}^{n+\frac{1}{2}} - v_{i,j-\frac{1}{2}}^{n+\frac{1}{2}}}{h}.$$

The resulting linear system (3.4) is solved using a multigrid method with Gauss-Seidel relaxation. Then the discrete divergence-free cell-edge velocities $\tilde{u}$ and $\tilde{v}$ are defined by

$$\tilde{u}_{i+\frac{1}{2},j}^{n+\frac{1}{2}} = u_{i+\frac{1}{2},j}^{n+\frac{1}{2}} - \frac{\phi_{i+1,j} - \phi_{ij}}{h}, \quad \tilde{v}_{i,j+\frac{1}{2}}^{n+\frac{1}{2}} = v_{i,j+\frac{1}{2}}^{n+\frac{1}{2}} - \frac{\phi_{i,j+1} - \phi_{ij}}{h}.$$

The convective terms are discretized as:

$$\begin{aligned}
(\mathbf{u} \cdot \nabla_d \mathbf{u})_{ij}^{n+\frac{1}{2}} &= \frac{\tilde{u}_{i+\frac{1}{2},j}^{n+\frac{1}{2}} + \tilde{u}_{i-\frac{1}{2},j}^{n+\frac{1}{2}}}{2h}(\bar{\mathbf{u}}_{i+\frac{1}{2},j}^{n+\frac{1}{2}} - \bar{\mathbf{u}}_{i-\frac{1}{2},j}^{n+\frac{1}{2}}) \\
&\quad + \frac{\tilde{v}_{i,j+\frac{1}{2}}^{n+\frac{1}{2}} + \tilde{v}_{i,j-\frac{1}{2}}^{n+\frac{1}{2}}}{2h}(\bar{\mathbf{u}}_{i,j+\frac{1}{2}}^{n+\frac{1}{2}} - \bar{\mathbf{u}}_{i,j-\frac{1}{2}}^{n+\frac{1}{2}}), \\
(\mathbf{u} \cdot \nabla_d \mathbf{c})_{ij}^{n+\frac{1}{2}} &= \frac{\tilde{u}_{i+\frac{1}{2},j}^{n+\frac{1}{2}} + \tilde{u}_{i-\frac{1}{2},j}^{n+\frac{1}{2}}}{2h}(\bar{\mathbf{c}}_{i+\frac{1}{2},j}^{n+\frac{1}{2}} - \bar{\mathbf{c}}_{i-\frac{1}{2},j}^{n+\frac{1}{2}}) \\
&\quad + \frac{\tilde{v}_{i,j+\frac{1}{2}}^{n+\frac{1}{2}} + \tilde{v}_{i,j-\frac{1}{2}}^{n+\frac{1}{2}}}{2h}(\bar{\mathbf{c}}_{i,j+\frac{1}{2}}^{n+\frac{1}{2}} - \bar{\mathbf{c}}_{i,j-\frac{1}{2}}^{n+\frac{1}{2}}),
\end{aligned}$$

where the edge values $\bar{\mathbf{c}}_{i\pm\frac{1}{2},j}^{n+\frac{1}{2}}$, $\bar{\mathbf{u}}_{i\pm\frac{1}{2},j}^{n+\frac{1}{2}}$, $\bar{\mathbf{c}}_{i,j\pm\frac{1}{2}}^{n+\frac{1}{2}}$, and $\bar{\mathbf{u}}_{i,j\pm\frac{1}{2}}^{n+\frac{1}{2}}$ are computed using projected velocity fields, $\tilde{u}$, $\tilde{v}$, and a fifth order WENO algorithm [24].

3.2. Discretization of surface tension terms. In this section we describe the finite difference approximation to the surface tension term, $\mathbf{F}_{st}$. Let

$$\begin{aligned}
\mathbf{F}_{st} &= -\sum_{k=1}^{3} \frac{\epsilon\beta}{We_k}(f_k, g_k) = \sum_{k=1}^{3} \frac{\epsilon\beta}{We_k} \nabla \cdot (|\nabla c_k|^2 I - \nabla c_k \otimes \nabla c_k) \\
&= -\sum_{k=1}^{3} \frac{\epsilon\beta}{We_k}(\partial_x c_k \partial_{yy} c_k - \partial_y c_k \partial_{xy} c_k,\ \partial_y c_k \partial_{xx} c_k - \partial_x c_k \partial_{xy} c_k).
\end{aligned}$$

Then, the surface tension force components (f_1, g_1) are discretized as

$$(f_1)_{ij} = \frac{1}{2h^3}(c_{1\,i+1,j} - c_{1\,i-1,j})(c_{1\,i,j+1} - 2c_{1\,ij} + c_{1\,i,j-1}) \tag{3.5}$$
$$-\frac{1}{8h^3}(c_{1\,i,j+1} - c_{1\,i,j-1})(c_{1\,i+1,j+1} + c_{1\,i-1,j-1} - c_{1\,i+1,j-1} - c_{1\,i-1,j+1})$$
$$(g_1)_{ij} = \frac{1}{2h^3}(c_{1\,i,j+1} - c_{1\,i,j-1})(c_{1\,i+1,j} - 2c_{1\,ij} + c_{1\,i-1,j}) \tag{3.6}$$
$$-\frac{1}{8h^3}(c_{1\,i+1,j} - c_{1\,i-1,j})(c_{1\,i+1,j+1} + c_{1\,i-1,j-1} - c_{1\,i+1,j-1} - c_{1\,i-1,j+1})$$

and the other components, (f_2, g_2) and (f_3, g_3), are similarly defined by replacing c_1 in Eqs. (3.5) and (3.6) by c_2 and $1 - c_1 - c_2$, respectively. Further, $\mathbf{F}_{st}^{n+\frac{1}{2}}$ in Eq. (3.3) is evaluated using $\mathbf{c}^{n+\frac{1}{2}} = (\mathbf{c}^n + \mathbf{c}^{n+1})/2$.

4. Numerical experiments. In this section, we demonstrate convergence of our scheme numerically and simulate a three-phase contact angle, a buoyancy-driven compound drop, and liquid/liquid remediation enhanced by the Rayleigh-Taylor instability.

4.1. Convergence test. To obtain an estimate of the rate of convergence, we perform a number of simulations for a sample initial problem on a set of increasingly finer grids. The initial data is

$$c_1(x,y,0) = \frac{1}{2}\left(1 - \tanh\left(\frac{y-\frac{1}{3}}{2\sqrt{2}\epsilon}\right)\right), \quad c_2(x,y,0) = \frac{1}{2}\left(\tanh\left(\frac{y-\frac{1}{3}}{2\sqrt{2}\epsilon}\right) - \tanh\left(\frac{y-\frac{2}{3}}{2\sqrt{2}\epsilon}\right)\right)$$

That is, narrow transition layers separate three immiscible fluids. The initial velocity is a swirling flow

$$u(x,y,0) = -0.25\sin^2(\pi x)\sin(2\pi y), \quad v(x,y,0) = 0.25\sin^2(\pi y)\sin(2\pi x)$$

on a domain, $\Omega = (0,1)\times(0,1)$. No-slip boundary conditions are applied to top and bottom planes and periodic ones are to the side walls. The numerical solutions are computed on the uniform grids, $h = 1/2^n$ for $n = 5, 6, 7, 8,$ and 9. For each case, the calculations are run to time $T = 0.2$, the uniform time steps, $\Delta t = 0.1h$, $Re = 10$, $We_1 = We_2 = We_3 = 100$, $Pe = 2$, and $\epsilon = 0.005\sqrt{2}$, are used to establish the convergence rates.

TABLE 4.1
Convergence Results — $u, v, c_1,$ and c_2.

Case	32-64	64-128	rate	128-256	rate	256-512	rate
u	5.4530e-4	4.4986e-5	3.5995	1.0895e-5	2.0458	2.7798e-6	1.9706
v	6.8462e-4	2.9858e-5	4.5191	7.5194e-6	1.9894	1.8850e-6	1.9961
c_1	2.9211e-2	3.1969e-3	3.1918	7.5863e-4	2.0752	1.8755e-4	2.0161
c_2	4.1640e-2	4.2759e-3	3.2836	1.0037e-3	2.0908	2.4801e-4	2.0169

Since a cell centered grid is used, we define the error to be the difference between that grid and the average of the next finer grid cells covering it:

$$e_{h/\frac{h}{2}\,ij} \stackrel{def}{=} c_{hij} - \left(c_{\frac{h}{2}\,2i,2j} + c_{\frac{h}{2}\,2i-1,2j} + c_{\frac{h}{2}\,2i,2j-1} + c_{\frac{h}{2}\,2i-1,2j-1}\right)/4.$$

The rate of convergence is defined as the ratio of successive errors in the discrete l_2-norm:

$$\log_2(||e_{h/\frac{h}{2}}||/||e_{\frac{h}{2}/\frac{h}{4}}||).$$

The errors and rates of convergence are given in table 4.1. The results suggest that the scheme is indeed second order accurate.

4.2. Contact angles. Following [26], we next investigate the spreading of a liquid lens consisting of an initially circular immiscible droplet of fluid located at an interface between two other immiscible fluids. See Fig 4.1(a).

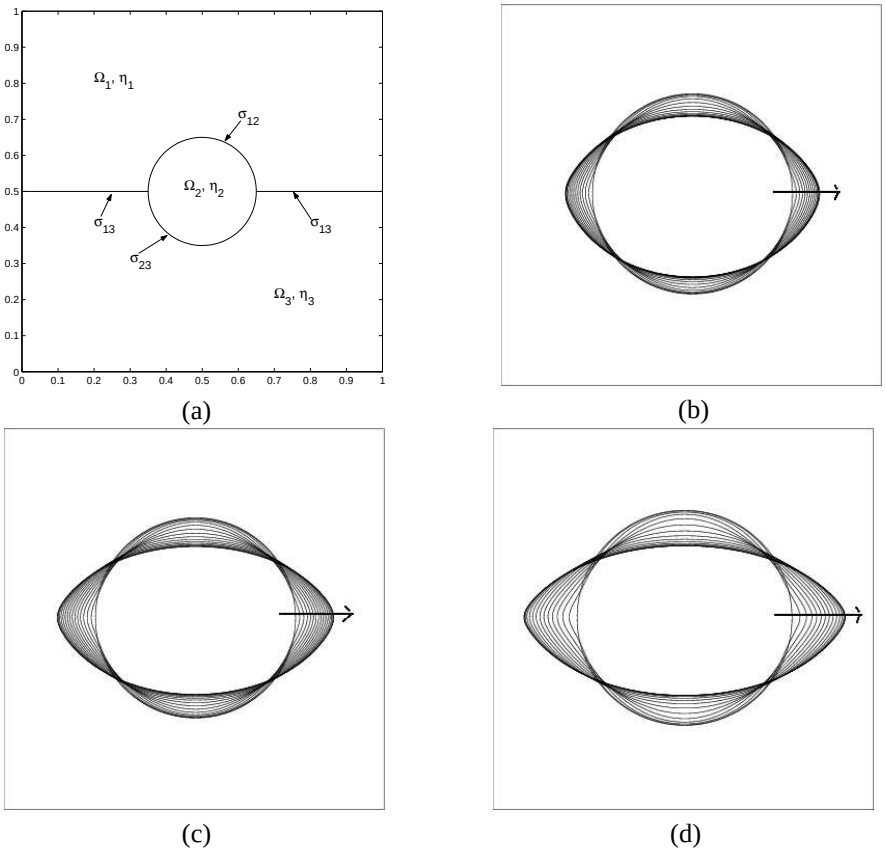

FIG. 4.1. *(a) Initial configuration: the upper fluid is phase 1, the lower fluid is phase 3, and the droplet is phase 2. (b), (c), and (d) are evolutions of initial circular drop for* $We_2 = 60$ *and* $We_1 = We_3 = 108,\ 60,\ 36$, *respectively. The arrow shows the direction of the evolution and the most deformed lines in (b), (c), and (d) are corresponding steady shapes and the enclosing box size is* $[0.23, 0.77] \times [0.23, 0.77]$.

The initial condition is a circular droplet, Ω_2, (located at a free surface between Ω_1 and Ω_3) and the initial velocity is zero, i.e.,

$$\begin{aligned}
c_1(x,y,0) &= \max\left[0.5\left(1+\tanh\left(\frac{y-0.5}{2\sqrt{2}\epsilon}\right)\right) - c_2(x,y), 0\right], \\
c_2(x,y,0) &= 0.5\left(1+\tanh\left(\frac{0.15-\sqrt{(x-0.5)^2+(y-0.5)^2}}{2\sqrt{2}\epsilon}\right)\right), \\
u(x,y,0) &= v(x,y,0) = 0.
\end{aligned}$$

The computational domain is $\Omega = [0,1]\times[0,1]$. The fluids are density and viscosity matched ($\rho = 1,\ \eta = 1$) and

$$Re = 60, \text{ and } We_2 = 60, We_1 = We_3 = 108,\ 60,\ 36.$$

In Figs. 4.1(b)-(d), the evolution of the $c_2 = 1/2$ contour line is shown for three cases with $Re = 60$, and $We_2 = 60, We_1 = We_3 = 108,\ 60,\ 36$, respectively. In all cases, $\epsilon = 0.005\sqrt{2},\ \ Pe = 100/\epsilon$, $h = 1/256$, and $\Delta t = 0.25h$. As the droplet spreads, it reaches an equilibrium shape. The most deformed curve in each figure is the numerical steady-state. Theoretically, the shape of the steady-state drop is controlled by the drop-volume and the three surface tensions (inverse Weber numbers). The equilibrium three-phase contact angle is determined by

$$\frac{\sin\theta_1}{\frac{1}{We_2}+\frac{1}{We_3}} = \frac{\sin\theta_2}{\frac{1}{We_1}+\frac{1}{We_3}} = \frac{\sin\theta_3}{\frac{1}{We_1}+\frac{1}{We_2}}$$

and the relation between the lens area A, its length d (the distance between triple junctions), and the contact angles θ_i of the i-th phase (Young's law) is

$$d = \left(\frac{1}{8A}\left(\frac{2(\pi-\theta_1)-\sin(2(\pi-\theta_1))}{\sin^2(\pi-\theta_1)} + \frac{2(\pi-\theta_3)-\sin(2(\pi-\theta_3))}{\sin^2(\pi-\theta_3)}\right)\right)^{-\frac{1}{2}}.$$

Thus, the accuracy of the steady lens shape can be measured by comparing the observed d with the analytical value.

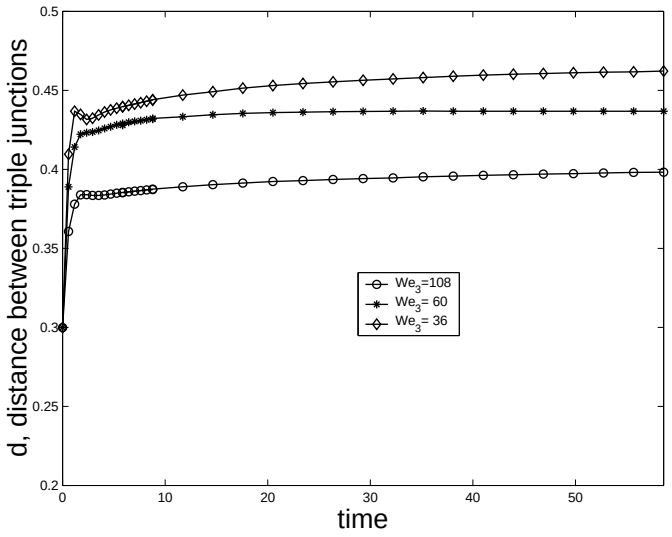

FIG. 4.2. *Time evolution of d, distance between triple junctions.* $We_3 = 108$ *(*$\circ$*),* $We_3 = 60$ *(*$*$*), and* $We_3 = 36$ *(*$\diamond$*).*

The evolution of d for the three cases is shown in Fig. 4.2. The numerical value of a d is obtained from the $c_2 = 1/2$ contour line. Note that in all cases, there is rapid increase in d at early times followed by a slow equilibrium process. Note also there is an overshoot in the early evolution of the $We_3 = 36$ and $We_3 = 108$ cases. In table 4.2, the equilibrium values of d are shown for the three cases together with the corresponding theoretical values. There is very good agreement between the theory and simulation.

TABLE 4.2
Equilibrium measurements

We_1, We_2, We_3	d_{exact}	$d_{numerical}$
108, 60, 108	0.3746	0.3982
60, 60, 60	0.4138	0.4368
36, 60, 36	0.4578	0.4622

Next, we consider a similar problem in three-dimensions. We place a periodic array of spheres on an interface between two immiscible fluids. Schematic is a three-dimensional analog to the two-dimensional one Fig. 4.1(a). The computational domain is $\Omega = [0,1] \times [0,1] \times [0,1]$ and the mesh size is $64 \times 64 \times 64$ with time step, $\Delta t = 0.001$. $\epsilon = 0.008\sqrt{2}$, and $Pe = 100/\epsilon$. No-slip boundary conditions for the top and bottom planes and periodic boundary conditions for side walls are applied. Specifi cally, the initial data in a single period box are

$$c_1(x,y,z) = \max\left[0.5\left(1+\tanh\left(\frac{z-0.5}{2\sqrt{2}\epsilon}\right)\right) - c_2(x,y), 0\right],$$
$$c_2(x,y,z) = 0.5\left(1+\tanh\left(\frac{0.35-\sqrt{(x-0.5)^2+(y-0.5)^2+(z-0.5)^2}}{2\sqrt{2}\epsilon}\right)\right),$$
$$u(x,y,z) = v(x,y,z) = w(x,y,z) = 0.$$

We take the viscosities and densities of the components to be matched $(\eta_1 = \eta_2 = \eta_3 = 1)$ and $(\rho_1 = \rho_2 = \rho_3 = 1)$ with the following parameters.

$$Re = 60,\ \ We_1 = We_3 = 36,\ We_2 = 60.$$

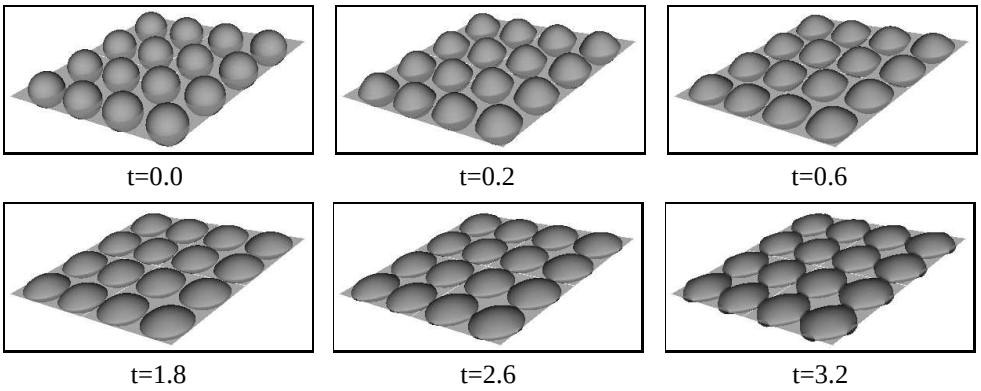

FIG. 4.3. *Evolution of spheres under surface tension forces, the nondimensional times are shown below each figure.*

In Fig. 4.3, evolution is shown and only the spheres are visualized with a reference plane passing through equator of the spheres. The actual interface deforms. As the drops spread out and flatten due to surface tension forces, the drops interact with their periodic neighbors. In this case, the distance between the neighbors is less than the equilibrium length of an

isolated drop. As seen in Fig. 4.3, this leads to merger with the periodic images and results in a lattice-like microstructure of the second fluid on the interface between the two other immiscible fluids.

4.3. Numerical simulation of a buoyancy-driven compound drop. In this section, a buoyancy-driven evolution a 3-D compound drop is investigated. In Fig. 4.4, a schematic of the initial configuration is shown. The three fluids are immiscible where a heavy droplet of fluid I is encapsulated by a light fluid II. Fluid I is the heaviest component. This models a flow in which a heavy fluid contains a dispersed contaminant. Releasing drops of the light fluid II from the bottom of the container, provides the means to encapsulate the contaminants. Restricting this to a single drop yields the initial condition we consider.

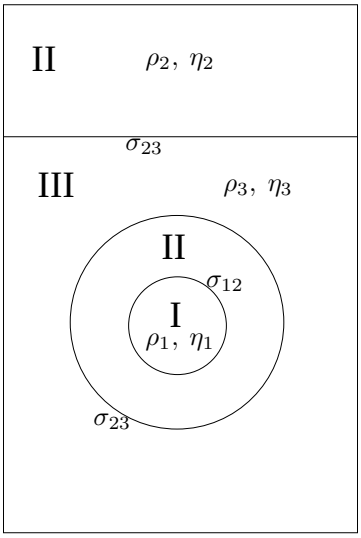

FIG. 4.4. *Schematic of a compound drop.*

Specifically, the initial data are

$$c_1(x,y,z) = 0.5\left(1+\tanh\left(\frac{0.3-r}{2\sqrt{2}\epsilon}\right)\right),$$
$$c_2(x,y,z) = 0.5\left(2+\tanh\left(\frac{0.5-r}{2\sqrt{2}\epsilon}\right)+\tanh\left(\frac{z-2.5}{2\sqrt{2}\epsilon}\right)\right)-c_1(x,y,z),$$
$$u(x,y,z) = v(x,y,z) = w(x,y,z) = 0,$$

where $r=\sqrt{(x-1)^2+(y-1)^2+(z-1.5)^2}$. We take the viscosities and surface tensions of the components to be matched ($\eta_1=\eta_2=\eta_3=1$) and ($\sigma_1=\sigma_2=\sigma_3=1$) with the following parameters.

$$\rho_1 = 1.044,\ \rho_2 = 0.957,\ \ \rho_3 = 1,\ Re = 36,\ We_1 = We_2 = We_3 = 1127,\ \text{and}\ Fr = 1.$$

The computational domain is $\Omega=[0,2]\times[0,2]\times[0,4]$ and the mesh size is $32\times32\times64$ with time step, $\Delta t = 0.002$. $\epsilon = 0.01\sqrt{2}$, and $Pe = 10/\epsilon$. No-slip boundary conditions for the top and bottom planes and periodic boundary conditions for the side walls are applied.

The evolution is presented in Fig. 4.5. An upper (flat) interface separates the heavy ambient from same fluid that encapsulates the heavy drop. The compound drop is lighter

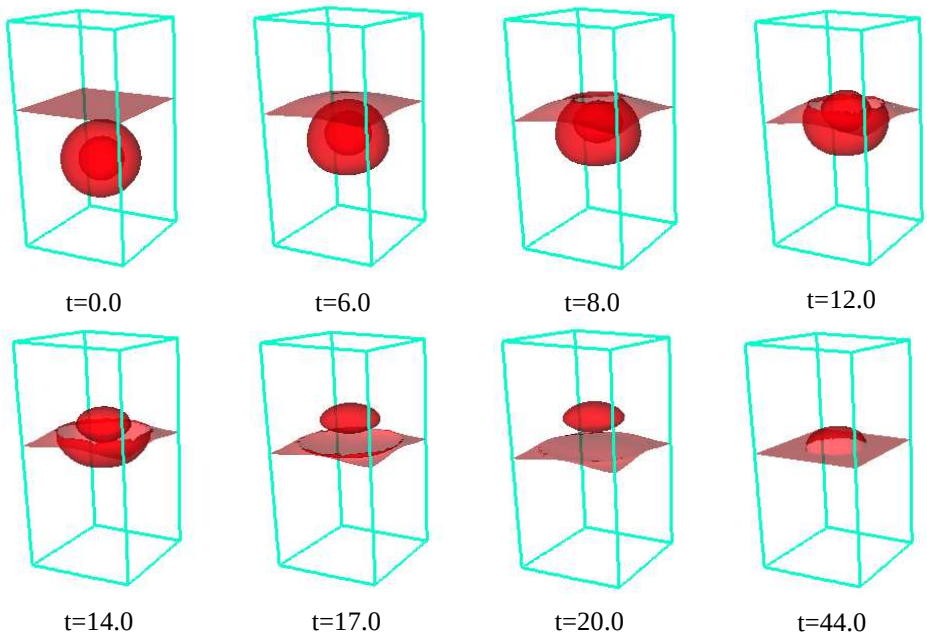

FIG. 4.5. *Evolution of a compound drop, the nondimensional times are shown below each figures.*

than the heavy ambient and so it rises and deforms. The encapsulating fluid rises faster than the heavy inner drop but nevertheless the compound drop remains intact until it penetrates the upper interface. The heavy inner drop is carried upwards as the encapsulated fluid is released. The drop then falls back on the interface remaining trapped there by surface tension forces even though if is heavier than the lower ambient. At this point, the drop could be removed from the system by "sucking" it off the interface. Imagining that the heavy inner drop is a contaminant in the lower ambient, this provides a mechanism of liquid/liquid extraction by which fluid III may be cleansed.

4.4. Rayleigh-Taylor Instability of Ternary Fluid Flows. In this section, we exploit the fact that our ternary NSCH system is capable of describing multicomponent fluid flows containing immiscible, miscible and partially miscible components. The miscibility of the components is modeled through the properties of the free energy $F(c_1, c_2)$. It is nontrivial to construct free energies capable of describing partially miscible systems where, for example, two components are immiscible and the third component is preferentially miscible in one of the immiscible components. Nevertheless, we have been able to construct a class of such a free energies and one example of which is given below:

$$F(c_1, c_2) = 2c_1^2(1 - c_1 - c_2)^2 + (c_1 + 0.2)(c_2 - 0.2)^2 + (1.2 - c_1 - c_2)(c_2 - 0.4)^2.$$

A contour plot of the free energy $F(c_1, c_2)$ on the Gibbs triangle is shown in Fig. 4.6. The two minima of $F(c_1, c_2)$ are at $(0.7779, 0.2330, -0.0109)$ and $(-0.0151, 0.3651, 0.6499)$. These minima lie very slightly outside the Gibbs triangle. As a demonstration of the evolution possible in partially miscible liquid systems, we present an example in which there is a gravity-driven (Rayleigh-Taylor) instability that enhances the transfer of a preferentially miscible contaminant from one immiscible fluid to another in 2D. The initial configuration is shown in Fig. 4.7. The top half of the domain consists of a mixture of fluid I and fluid II,

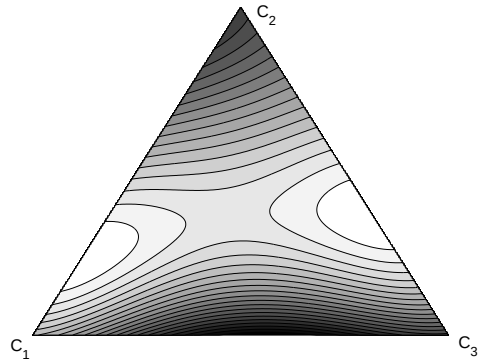

FIG. 4.6. *Contour plot of the free energy $F(c_1, c_2)$ on the Gibbs triangle.*

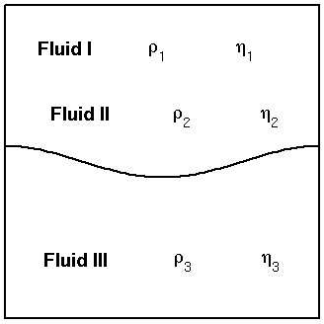

FIG. 4.7. *schematic of initial confi guration*

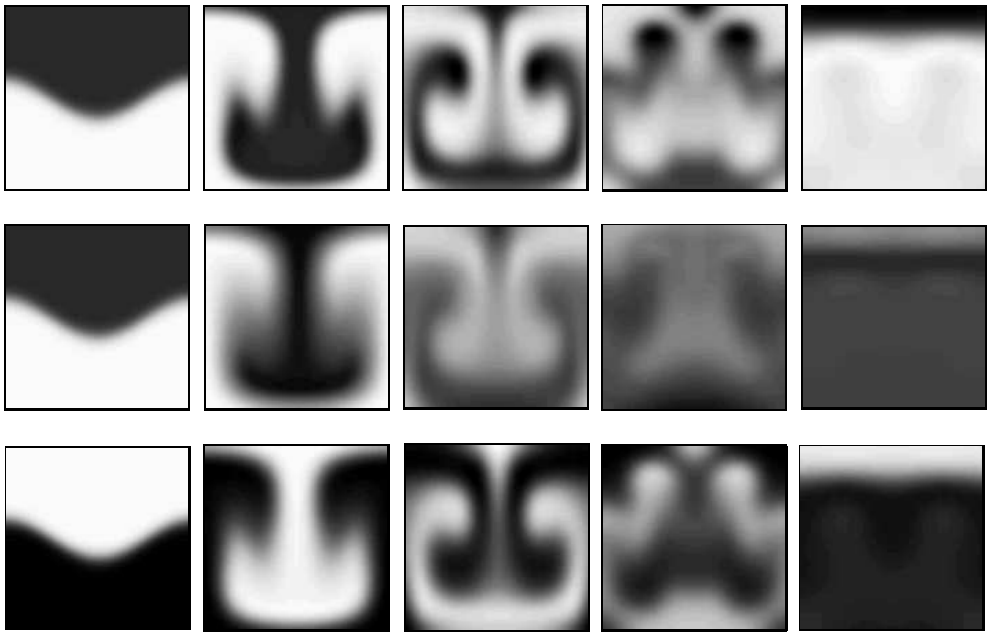

FIG. 4.8. *Evolution of concentration of fluid I (top row), II (middle row), and III (bottom row). The contours of c_1, c_2, and c_3 are visualized in gray-scale where darker regions denote larger values of c_1, c_2, and c_3, respectively. Nondimensional times are t = 0.00, 4.69, 7.81, 14.06, and 156.25.*

and the bottom half consists of fluid III, which is immiscible with fluid I. Fluid II is preferentially miscible with fluid III. Fluid I is assumed to be the lightest and fluid II the heaviest. The density of the I/II mixture is heavier than that of fluid III, so the density gradient induces Rayleigh-Taylor Instability.

In particular, the initial data are

$$c_1(x,y) = c_2(x,y) = 0.25\left(1 + \tanh\left(\frac{y - 0.5 - 0.1\cos(2\pi x)}{2\sqrt{2}\epsilon}\right)\right)$$
$$u(x,y) = v(x,y) = 0$$

and the simulation parameters are

$$\rho_1 = 1,\ \rho_2 = 4,\ \rho_3 = 2,\ Fr = 1,\ Re = 313,\ We_1 = We_2 = We_3 = 9.8 \times 10^6.$$

The computational domain is $\Omega = [0,1] \times [0,1]$ and the mesh size is 64×64 with time step, $\Delta t = 0.1h$. $\epsilon = 0.015\sqrt{2}$ and $Pe = 10/\epsilon$. Here, we minimize the effect of surface tension to increase instability of the interface.

The evolution of the three phases is shown in Fig. 4.8. The top row shows the evolution of fluid I, middle and bottom correspond to fluid II and fluid III, respectively. That is, the contours of $c_1,\ c_2,$ and c_3 are visualized in gray-scale where darker regions denote larger values of $c_1,\ c_2,$ and c_3, respectively. As the simulation begins, the I/II mixture falls and fluid II diffuses into fluid III. A characteristic Rayleigh-Taylor (inverted) mushroom forms, the surface area of the I/III interface increases, and vorticity is generated and shed into the bulk. As fluid II is diffused from fluid I, the pure fluid I rises to the top as shown in Fig. 4.8. Imagining that fluid II is a contaminant in fluid I, this configuration provides an efficient means of cleansing fluid I since the buoyancy-driven flow enhances the diffusional transfer of fluid II from fluid I to fluid III.

5. Conclusion. In this paper we have presented a general model of three-phase flows and developed associated efficient, second-order accurate finite difference method to solve the model equations numerically. The three-liquid phases may be fully miscible, partially miscible or immiscible. The miscibility of the phases is modeled thermodynamically through the Helmholtz free energy. An additional advantage of the model is that triple interfaces are handled without resorting to ad-hoc procedures.

We presented examples of flow with miscible and immiscible components. We demonstrated the convergence of our algorithm through a resolution study. In addition, we found good agreement with the theory for an equilibrium liquid lens (lying atop an interface). We provided demonstrations of liquid/liquid remediation. In the first example, a compound drop was simulated, in which a light fluid encapsulated a heavy contaminant drop. The light fluid causes the compound drop to rise and deposit the contaminant at an interface where it may be removed. In the second example, we investigated the diffusional transfer of a preferentially miscible contaminant from one immiscible phase to another. The transfer is enhanced by the flow and in particular the Rayleigh-Taylor instability.

In future work, we will perform more extensive studies of liquid/liquid remediation. In addition, we will investigate the complex morphologies generated from the application of chaotic mixing flow to three-phase dispersion. Under appropriate conditions, a coalescence cascade ensures and the three-phases may become interpenetrating and continuous. We will also investigate the limit in which one of the phases lies on the boundary between the other phases, thus mimicking a surfactant.

Acknowledgments. The authors acknowledge the support of the Department of Energy, Office of Basic Energy Sciences and the National Science Foundation. The authors are also grateful for the support of the Minnesota Supercomputer Institute and the Network & Academic Computing Services (NACS) at UCI.

REFERENCES

[1] A. S. Almgren, J. B. Bell, and W. G. Szymczak, *A numerical method for the incompressible Navier-Stokes equations based on an approximate projection*, SIAM J. Sci. Comput. **17**, no. 2, 358 (1996).

[2] Ann S. Almgren, John B. Bell, Phillip Colella, Louis H. Howell, Michael L. Welcome, *A Conservative Adaptive Projection Method for the Variable Density Incompressible Navier-Stokes Equations*, J. Comput. Phys. **142**, no. 1, 1 (1998)

[3] D. Anderson, G.B. McFadden, and A.A. Wheeler, *Diffuse interface methods in fluid mechanics*, Ann. Rev. Fluid Mech., 30:139-165, 1998.
[4] J. Bell, P. Collela, and H. Glaz, A second-order projection method for the incompressible Navier-Stokes equations, J. Comp. Phys. 85 no. 2, (1989) 257-283.
[5] S. Chen, G.D. Doolen, *Lattice Boltzmann method for fluid flows*, Ann. Rev. Fluid Mech., 30:329-364, 1998.
[6] Cahn JW and Hilliard JE, *Free energy of a non-uniform system. I. Interfacial free energy*, J Chem Phys 1958;28:258-267.
[7] Y.C. Chang, T.Y. Hou, B. Merriman, and S. Osher, *A Level Set Formulation of Eulerian Interface Capturing Methods for Incompressible Fluid Flows*, J. Comput. Phys., 124(2):449-464, 1996.
[8] B.D. Coleman and W. Noll, *Thermodynamics of elastic materials with conduction and viscosity*, Arch. Rat. Mech. Anal. v. 13 (1963) 167.
[9] David Jacqmin, Contact-line dynamics of a diffuse fluid interface, J. Fluid Mech. 402 (2000) 57-88.
[10] J. Glimm, J.W. Grove, X. Li, K. Shyue, Y. Zeng, and Q. Zhang, *Three-Dimensional Front Tracking*, SIAM J. Sci. Comput., 19(3):703-727, 1998.
[11] D. Gueyffier, J. Li, A. Nadim, R. Scardovelli, and S. Zaleski, *Volume-of-Fluid Interface Tracking with Smoothed Surface Stress Methods for Three-Dimensional Flows*, J. Comput. Phys., 152(2):423-456, 1999.
[12] S.R. de Groot and P. Mazur, *Non-equilibrium thermodynamics*, Dover, 1984 (originally published by North-Holland, Amsterdam, 1962).
[13] T.Y. Hou, J.S. Lowengrub, and M.J. Shelley, *Boundary Integral Methods for Multicomponent Fluids and Multiphase Materials*, J. Comput. Phys., 169(2):302-362, 2001.
[14] P.C. Hohenberg and B.I. Halperin, *Theory of dynamic critical phenomena*, Rev. Mod. Phys. v. 49 (1977) 435.
[15] R.A. Johnson and A. Borhan, *Stability of the shape of a surfactant-laden drop translating at low Reynolds number*, Phys. Fluids 12, 773-784. (2000)
[16] G.S. Jiang and C.-W. Shu, *Efficient implementation of weighted ENO schemes*, J. Comput. Phys., 126(1):202-228, 1996.
[17] J.S. Kim, K. Kang, and J.S. Lowengrub, *Conservative multigrid methods for Cahn-Hilliard fluids*, J. Comput. Phys., 193(2):511-543, 2004.
[18] J.S. Kim, K. Kang, and J.S. Lowengrub, *Conservative multigrid methods for ternary Cahn-Hilliard systems*, Comm. Math. Sci., 2(1):53-77, 2004.
[19] H.C. KAN, H.S. UDAYKUMAR, W. SHYY, AND R. TRAN-SON-TAY, *Hydrodynamics of a compound drop with application to leukocyte modeling*, Phys. Fluids, 10 (1998), pp. 760-774.
[20] H.Y. Lee, J.S. Lowengrub and J. Goodman, *Modeling pinchoff and reconnection in a Hele-Shaw cell. I. The models and their calibration* , Phys. Fluids **14**, no. 2, 492 (2002).
[21] Lowengrub, J.; Truskinovsky, L., *Quasi-incompressible Cahn-Hilliard fluids and topological transitions.*, R. Soc. Lond. Proc. Ser. A Math. Phys. Eng. Sci. **454**, no. 1978, 2617 (1998).
[22] Peskin, C. S., *Numerical analysis of blood flow in the heart*, J. Comput. Phys. 25:220252, 1977.
[23] D.A. PORTER AND K.E. EASTERLING, *Phase Transformations in Metals and Alloys*, van Nostrand Reinhold, 1993.
[24] S. Zheng, *Asymptotic behavior of the solution to the Cahn-Hilliard equation*, Applic. Anal. **23**, 165 (1986).
[25] M. Sussman, Puckett, G. Elbridge, A coupled level set and volume-of-fluid method for computing 3D and axisymmetric incompressible two-phase flows, J. Comput. Phys. 162 no. 2, (2000) 301-337.
[26] K.A. Smith, F.J. Solis, D.L. Chopp, A projection method for motion of triple junctions by levels sets, Interfaces Free Bound. **4** (2002), no. 3, pp. 263-276.
[27] G. Tryggvason, B. Bunner, A. Esmaeeli, D. Juric, N. Al-Rawahi, W. Tauber, J. Han, S. Nas and Y. -J. Jan, *A Front-Tracking Method for the Computations of Multiphase Flow*, J. Comput. Phys., 169(2):708-759, 2001.
[28] C. Truesdell and W. Noll, *The nonlinear field theories of mechanics*, In The Encyclopedia of Physics. Ed. (S. Flugge), vol III. Springer-Verlag. 1965.
[29] I.T. TAI AND A.M. SUN, *Microencapsulation of recombinant cells: a new delivery system for gene therapy*, FASEB J., 7 (1993), pp. 1061-1069.
[30] H.S. Udaykumar, H.-C. Kan, W. Shyy, and R. Tran-Son-Tay, *Multiphase dynamics in arbitrary geometries on fixed Cartesian grids*, J. Comput. Phys., 137:366-405, 1997.